Atmos. Chem. Phys. Discuss., https://doi.org/10.5194/acp-2018-440
Manuscript under review for journal Atmos. Chem. Phys.
Discussion started: 4 June 2018

Atmospheric Chemistry and Physics Discussions

Ground-based MAX-DOAS observations of tropospheric formaldehyde and comparisons with CAMS model at a rural site near Beijing

Xin Tian [1,2], Pinhua Xie *[1,2,4], Jin Xu *[2], Yang Wang *[3], Ang Li [2], Fengcheng Wu [2], Zhaokun Hu [2], Cheng Liu[2,4,5,6], Qiong Zhang [2]

1. School of Environmental Science and Optoeclectronic Technology, University of Science and Technology of China, Hefei, 230026,China;
2. Key laboratory of Environmental Optical and Technology, Anhui Institute of optics and Fine Mechanies, Chinese Academy of Science, Hefei, 230031,China;
3. Max Planck Institute for Chemistry, Mainz, 55128, Germany;
4. CAS Center for Excellence in Urban Atmospheric Environment, Institute of Urban Environment, Chinese Academy of Sciences, Xiamen, 361021, China;
5. School of Earth and Space Sciences, University of Science and Technology of China, Hefei, 230026, China;
6. Anhui Province Key Laboratory of Polar Environment and Global Change, USTC, Hefei, 230026, China;
Correspondence to: Xin Tian (xtian@aiofm.ac.cn); Pinhua Xie (phxie@aiofm.ac.cn); Jin Xu (jxu@aiofm.ac.cn); Yang Wang (y.wang@mpic.de)

Abstract. Formaldehyde (HCHO), a key aerosol precursor, plays a significant role in atmospheric photo-oxidation pathways. In this study, HCHO column densities were measured using Multi-axis Differential Optical Absorption Spectroscopy (MAX-DOAS) instrument at the University of Chinese Academy of Science (UCAS) in Huairou District, Beijing, which is about 50 km away from the city center, during the period of October 1, 2014 to December 31, 2014, in which the Asia-Pacific Economic Cooperation (APEC) summit was organized on 3 to 12 November. Peak values of HCHO vertical column densities (VCDs) around noon and a good correlation coefficient of 0.87 between HCHO and O_3 indicate that the secondary sources of HCHO through photochemical reactions of volatile organic compounds (VOCs) dominate HCHO values in the area around UCAS. Dependences of HCHO VCDs on wind fields and backward trajectories were identified and indicated that the HCHO values in the area around UCAS were considerably affected by the transports of pollutants (VOCs) from polluted area in the south. The effects of control measures on HCHO VCDs during the APEC period were evaluated. During the period of APEC conference, the averaged HCHO is 37.95% and 30.75% lower than that during the pre-APEC and post-APEC period, respectively. The phenomenon could be attributed to both effects of prevailing northwest wind fields

during the APEC and strict control measures. We also compared the MAX-DOAS results with the Copernicus Atmosphere Monitoring Service (CAMS) model. The CAMS model and MAX-DOAS results are generally consistent with a good correlation coefficient of ~ 0.83. The peak values are well consistently captured by both data sets, but the low values are systematically underestimated by the CAMS model. The finding indicates the CAMS model can well simulate the effects of transports and the secondary sources of HCHO, but underestimate the local primary sources.

1 Introduction

The 2014 Asia-Pacific Economic Cooperation (APEC) conference was held in Huairou District of Beijing city. To improve the air quality in Beijing city during the APEC conference, the collaboration group of atmospheric pollution prevention and control in Beijing-Tianjin-Hebei (Jing-Jin-Ji) region and surrounding areas compiled the 《The APEC conference air quality assurance policy》(Liu et al., 2015). Some provinces, including Beijing, Tianjin, Hebei, Shanxi, Inner Mongolia, and Shandong provinces, implemented different emission reduction measurements in accordance with the air quality assurance plan (Wang et al., 2016). From November 1 to November 12, 2014, the air quality was at excellent level, which was known as "APEC blue."

At present, many studies analyzed the effects produced by emission reduction measures during the APEC summit. Wang et al., (2016) demonstrates that emission reduction measures in Beijing decreased SO_2, NO_2, PM_{10} and $PM_{2.5}$ concentrations by 74.1%, 48.0%, 66.6%, and 64.7%, respectively, whereas O_3 rose to 189.2%. Although the traffic and urban station created enormous pollution due to the emission of motor vehicles, the NO_2 concentrations of suburban and regional stations significantly dropped compared with the traffic and urban stations due to the control measures. The NO_2 emitted by motor vehicles in Beijing urban area remained high even under the measures to limit the number of vehicles. The CO, NOx, HC, and PM from exhaust emissions of motor vehicles decreased by 37.5%, 43.4%, 39.9%, and 42.9%, respectively (Fan et al., 2016). The analytical results of the Chemical Mass Balance (CMB) model showed that the emissions from coal-fired boiler, dust, and motor vehicles were around 2%, 7%, and 30% during the APEC summit (Cheng et al., 2016). $PM_{2.5}$ concentration during the control period decreased from 65.1% to 51.6% (Wang et al., 2017a). Zhang et al., (2017) analyzed the characteristics of aerosol size distribution and profile of vertical backscattering coefficient during the 2014 APEC summit

using lidar observation. Published studies focused mainly on the effects of commonly measured gas pollutants, PM, and aerosol, but not HCHO.

As an abundant product of the oxidation of many volatile organic compounds (VOCs), HCHO is known to harm human health, such as damage to oral epithelial cells (Nilsson et al., 1998; Pinardi et al., 2013). A variety of other hydrocarbons generally determine the concentration of HCHO. Thus, HCHO is used as an indicator of VOCs (Fried et al., 2011).

Troposphere formaldehyde comes from two sources. The primary emissions from incomplete combustion, such as anthropogenic (e.g., industrial emissions) and pyrogenic (mainly biomass burning) sources. The secondary sources come from the photo-oxidation process of many VOCs. In addition, a small fraction of HCHO is from direct emissions of biogenic sources (e.g., vegetation). The variability of HCHO over continents is particularly dominated by distributions of local emissions of non-methane volatile organic compounds (NMVOCs) (Chance et al., 2000). Although HCHO has a short lifetime, long-living VOCs, such as methane (CH_4), contribute to the background levels of HCHO (Vrekoussis et al., 2010). The monitoring NMVOC emissions is essential not only for the hydroxyl radical OH, but also for the formation and transport of secondary organic aerosols (Palmer et al., 2006; Stavrakou et al., 2009; De Smedt et al., 2015). HCHO is an important indicator of atmospheric photochemical reaction. As an active gas, HCHO can be photolyzed to generate HO_2- free radicals. HO_2 rapidly and radically reacts with NO to generate OH−, which can influence the oxidation ability of the atmosphere. Therefore, identifying the major sources of HCHO is essential for quantifying their contributions to aerosol formations and effectively controlling photochemical pollution. Implementing a series of temporary reduction measures for atmospheric pollutants emission in major international events in China is relatively rare. The APEC summits provide an opportunity for us to study the relationship between the environmental concentrations with pollutant emissions (Cheng et al., 2016). Therefore, studying the influences of control measures on HCHO is crucial to improve the air.

A kind of passive differential optical absorption spectroscopy system, called as MAX-DOAS, was used in the past decade to measure tropospheric trace gases (Nninger et al., 2004; Wagner et al., 2004; Sinreich et al., 2005; Wagner et al., 2007; Vigouroux wt al., 2009). The information obtained from MAX-DOAS measurements includes tropospheric column concentrations, surface concentrations, and vertical profiles. HCHO can be measured in the ultraviolet spectral range by a use of the MAX-DOAS technique (Vigouroux et al., 2009; Wagner et al., 2011; Pinardi et al., 2012, 2013; Li et al., 2013;

Atmos. Chem. Phys. Discuss., https://doi.org/10.5194/acp-2018-440
Manuscript under review for journal Atmos. Chem. Phys.
Discussion started: 4 June 2018

Borovski et al., 2014; Cheung et al., 2014; Franco et al., 2015; Lee et al., 2015; Schreier et al., 2016; Wang et al., 2017b; Wang et al., 2017c) .

In this study, we used the ground-based MAX-DOAS instrument installed in Huairou District (suburban area) of Beijing city to evaluate the effects of the emission control measures on HCHO from October 26, 2014 to November 20, 2014. The daily variation, transport, source, and the effect of APEC emission control measures of HCHO were analyzed. The relationships between HCHO VCDs and wind fields were analyzed. The HCHO VCDs retrieved from the MAX-DOAS measurements were then compared with the results from the CAMS model simulations from October 1, 2014 to December 31, 2014. Consistencies and discrepancies between model and measurements are discussed. This study can be used as reference in evaluating the effectiveness of photochemical pollution control measures adopted during the APEC summit. Moreover, this study could practically help the development of control strategies in the future. And it can also provide the support for verifying the model simulations.

2 Methodology

2.1 MAX-DOAS Methodology

MAX-DOAS, which is an optical remote-sensing technology and record spectra of scattered sunlight at different elevation angles, can be used to quantitatively measure trace gases based on Lambert Beer's Law (Hönninger and Platt, 2002; Bobrowski wt al., 2013; Roozendael et al., 2003; Trebs et al., 2004; Hönninger et al., 2004; Wagner et al., 2004). In the first step, the differential slant column densities (DSCDs) are derived by the DOAS spectral analysis with a so called Fraunhofer Reference Spectrum (FRS, measured in a small sun zenith angle at 90 ° elevation around noon) (Hermans et al., 2003; Hönninger and Platt, 2002; Kraus, 2006). Vertical column density (VCD) is defined as the integrated concentration of trace gas concentration through the atmosphere along the vertical path, and is calculated from dSCD by a use of air mass factor (AMF) as follows:

$$\mathrm{VCD} = \frac{dSCD_{\alpha \neq 90^\circ} - dSCD_{\alpha = 90^\circ}}{\mathrm{AMF}_{\alpha \neq 90^\circ} - \mathrm{AMF}_{\alpha = 90^\circ}} = \frac{\Delta \mathrm{SCD}}{\Delta \mathrm{AMF}}. \quad (1)$$

AMF is often used to describe the absorption path of a gas in the atmosphere. Brinksma et al., (2008) proposed the geometric

Atmos. Chem. Phys. Discuss., https://doi.org/10.5194/acp-2018-440
Manuscript under review for journal Atmos. Chem. Phys.
Discussion started: 4 June 2018

approximation method to calculate AMF:

$$AMF(\alpha) = 1/\sin\alpha \,. \qquad (2)$$

Numerous studies compared the error between geometrical VCD and VCD from profile inversion (Brinksma et al., 2008; Nninger wt al., 2004; Hendrick et al., 2014; Hönninger et al., 2004; Wang et al., 2017b). Wang et al., (2017b) showed that the geometric approximation are usually underestimate 10% than profile inversion for HCHO VCDs at 20 °elevation, but the error is larger for lager elevation angles and larger relative azimuth angle (RAA). This study uses the geometric approximation method to determine HCHO VCDs at an elevation angle of 15 °to avoid surface obstacles on light paths along the line of sight. Meanwhile, it has lower systematic errors because of the geometrical approximation. Besides the geometric approximation method is more stable and less influenced by the clouds than the profile inversion. (Hönninger et al., 2004; Clémer et al., 2010; Wagner et al., 2009; Wagner et al., 2011; Erle et al., 2013).

2.2 Monitoring locations

To evaluate the emission control measures, a supersite was established in the Yanqi Lake campus of the University of Chinese Academy of Sciences (UCAS) in Huairou District, northeast suburban area of Beijing, and the APEC conference also held in the Yanqi Lake near the campus of UCAS (**Fig.1)**. The field campaign was performed for nearly four months from October 1, 2014 and January 20, 2015. However, this study only discusses the period from October 2014 to December 2014.

The Yanshan Mountains are in the west of the site, and the Yanqi Lake lies at the edge of the Mountains in the southwest of the site. Beijing urban areas are also located in the south. Thus, air flow coming from south may bring anthropogenic emissions. The site is mainly influenced by emission from vehicles on China National Highway 111 that runs the north and south and some point sources along the highway (Zhang et al., 2017).

2.3 MAX-DOAS instrument and measurement

Fig. 2 shows the structural representation of the MAX-DOAS system. This system comprises a telescope, stepping motor,

spectrometer, and computer. Sunlight is focused by the telescope, which is installed outdoor and reaches the spectrometer through an optical fiber. The spectrometer is placed in a temperature-controlled box at 20 ℃. The spectrometer covers the range of 290 nm to 420 nm, and its instrumental function is approximated as a Gaussian function with a full width at half maximum (FWHM) of 0.5 nm.

The MAX-DOAS instrument was deployed on the balcony (without a roof) of a classroom on the 4th floor in the laboratory building in the campus of UCAS (116.67 ℃, 40.4 ℃) in the northeast suburban of Beijing. MAX-DOAS was routinely operated for 24 hours. Due to intensity of sunlight, only the daytime measurements are used for analysis. The night time measurements could be used to correct the dark current and offset. The azimuth angle view of the telescope is fixed at 0 ° (North) during the whole observation period. A full MAX-DOAS scan comprises six elevation angles (EA) (3, 5, 10, 15, 30, and 90 °) and lasts for approximately 10 min (see **Fig. 3**). Each measurement has an average of 100 scanning times, and integration time is adjusted automatically based on light intensity. **Table 1** lists the detailed setup of MAX-DOAS instrument.

2.4 DOAS analysis

The spectra obtained from MAX-DOAS are analyzed using WINDOAS software (Hermans et al., 2003). The fitting range is from 335 nm to 360 nm. The gas cross-sections of HCHO, BrO, NO_2, O_3, and O_4 are included in the fit. A spectrum at the 90 ° EA recorded at 12:09 local time (LT) on November 6, 2014 is used as the Fraunhofer reference spectrum (FRS) for all the retrievals. The ring structure (Fish and Jones, 2013), which is used to account for rotational Raman scattering effects, is calculated using Doasis software (Kraus, 2006) based on the FRS and included in the fit. **Table 2** lists the parameter settings used for the HCHO analysis.

Fig. 4 shows an example of the DOAS spectrum analysis in evaluating the HCHO slant column densities at 12:30 on November 19, 2014. The red and blue curves indicate the fitted absorption structures and the derived absorption structures from the measured spectra, respectively. HCHO SCD is 7.21×10^{16} molecules cm^{-2}. The root mean square of the residual error is 1.08×10^{-3}.

2.5 ECMWF CAMS model

The European Centre for Medium-Range Weather Forecasting (ECMWF) is at the forefront of research for numerical weather prediction including probabilistic forecasting. The Copernicus Atmosphere Monitoring Service (CAMS), which is managed by ECMWF, publicly provides the generally reliable information about the atmosphere. CAMS model is established utilizing the wealth of Earth observation data from satellite and ground-based systems. CAMS model produces real-time analyses and forecasts of atmospheric composition for the global view for each day (Persson and Grazzini, 2001). CAMS real-time products can be freely downloaded via a platform (http://apps.ecmwf.int/datasets/data/cams-nrealtime/levtype=sfc/) (Anders, 2015). The operational CAMS uses fully integrated chemistry in Composition Integrated Forecasting System (C-IFS). C-IFS is a new global chemistry model for forecast and assimilation of atmospheric composition. In the simulation of HCHO, chemistry originating from the TM5 CTM, had been fully integrated into the C-IFS, in which only gas phase reactions of HCHO are included. The actual emission totals used in the T255 simulation for 2008 from anthropogenic, biogenic sources and biomass burning were used in C-IFS (Flemming et al., 2014). All analyzed parameters acquired from the CAMS model are at 00, 06, 12, and 18 UTC. We use the CAMS model data with grid resolutions of 0.125 °× 0.125 °, 0.25 °× 0.25 °, and 0. 5 °× 0. 5 °at 8:00 LT (00:00 UTC) and 14:00 LT (06:00 UTC).

2.6 Meteorology data

Meteorological parameters, wind speed (WS), wind direction (WD), temperature (T), and relative humidity (RH) were continuously measured at the UCAS superstation from October 28, 2014 to December 31, 2014 (**Fig. 5a**). All measured meteorological parameters are averaged to 1 min time intervals. During the campaign, the temperature showed clearly diurnal variation of maximum at noon and minimum at night. The temperature was within a range of -10.59 ℃ to 20.7 ℃ with a suddenly drop to below 0 ℃ on December 1, 2014. Wind rose indicates that the prevailing wind direction was from northwest (**Fig. 5b**). The static weather situation (Halfacre et al., 2014) with a wind speed less than 3.5 m s^{-1}. frequently occurred. And the wind speeds of more than 3.5 m s^{-1} usually appeared under the northwest and west wind.

Atmos. Chem. Phys. Discuss., https://doi.org/10.5194/acp-2018-440
Manuscript under review for journal Atmos. Chem. Phys.
Discussion started: 4 June 2018

3 Results and discussion

In this session we evaluate the impact of emission control policy on air quality during APEC based on the MAX-DOAS measurements from the period of October 26, 2014 to November 20, 2014. Because the measurement station is at a rural site with a distance of about 50km away from the Beijing downtown area, wind fields, namely transports of pollutants, are considered in the evaluation. And the MAX-DOAS and CAMS model are compared to verify model data using the period of October 1, 2014 to December 31, 2014. Since a daytime period is relatively short in autumn, the available MAX-DOAS measurement time is from 06:30 to 18:30.

3.1 Effects of transports of pollutants

Fig. 6 shows the time series of HCHO VCDs measured by MAX-DOAS and meteorological parameters in the period of 3 to 8 November, 2014. Two peak values (November 4, 2014 and November 7, 2014) were observed during APEC **(Fig. 6a and 6f)**. Relative humidity, intensity of solar radiation, and ambient temperature are the important factors of photo-oxidation (Starn et al., 1998; Solberg et al., 2001; Zhang et al., 2009). The solar radiation and temperature were not significant changes at the two peaks process of November 4, 2014 and 7, 2014; thus, the enhanced HCHO values should not be caused by an increasing photo-oxidation rate. The increase of HCHO is probably related to a change of wind direction to south. **Fig. 6** presents wind speed increases and is more than 2.0 m s^{-1}. The south air flow is dominant during the two days with peak values of HCHO during the APEC summit. At noontime on November 3, 4, and 7, the wind direction changed to south and wind speed was relatively strong (approximately 4.0 m s^{-1}), thereby leading to a rapid accumulation of HCHO in a few hours. Thereafter, wind direction changed to northwest and wind speed became less than 2.0 m s^{-1} at the nighttime with the pollution gradually dissipated, which indicates that the contamination of supersite is affected by the pollution transports from the southwest areas. And the valley value on November 6, 2014 should be caused by the good dispersion conditions under northwest winds with a speed of more than 3.5 m s^{-1}.

To further demonstrate the effect of regional transports, we performed analysis of 24-h backward trajectories of air mass using the National Oceanic and Atmospheric Administration Hybrid Single Particle Lagrangian Integrated Trajectory (http://ready.arl.noaa.gov/HYSPLIT.php) on November 4 to 7, 2014 (**Fig. 7**). We used the 8:00 LT (UTC 0:00) as the start

time of backward trajectories. As shown in **Fig. 7**, pollutants over the polluted region, including Shijiazhuang and Baoding, in the southwest of Beijing, can be transported to the observed area on November 4, 2014. And the observed area was mainly affected by the pollution in Tangshan and Langfang located in the south and southeast of Beijing on November 7, 2014. Under the dominant northwest wind (November 5 to 6, 2014), the concentrations of HCHO were significantly lower than that on November 4 and 7, 2014, and reached the minimum under the high wind speed of up to 7.0 m s^{-1}. The change of dominant wind fields play important roles in the changes of HCHO at UCAS. Regional transport from the south has a significant impact on the increase of HCHO observed at the site.

We further analyze the relationship between HCHO VCDs and wind direction and speed from October 28, 2014 to November 20, 2014 in **Fig. 8**. Both local emission and transports from remote sources can impact observed HCHO VCDs. The main wind directions of the UCAS site are east, south, and northwest with approximate percentages of 16.5%, 16%, 12%, respectively. The amount of HCHO VCDs is strongly dependent on the wind speed and direction **(Fig. 8).** HCHO VCDs considerably depend on wind directions and the averaged HCHO VCDs are 7.57 $\times 10^{15}$ molecules cm^{-2} under the southerly wind (including southwest and southeast). This finding can be attributed to the fact that Tangshan, Baoding, Shijiazhuang and Tianjin, and other heavily polluted cities are located in the south of UCAS, including the city center of Beijing. By contrast, the northeast and north directions correspond to a minimum in HCHO VCDs, which are 6.64 $\times 10^{15}$ molec cm^{-2} on average. The wind from this area prominently contributes to the dispersion of the pollutants. In terms of the dependence of HCHO on wind speed, the HCHO VCDs decrease along the increasing wind speed under the northerly wind. And under the southerly wind, the HCHO VCDs increase with the increasing wind speed. In conclusion, when winds are from the south, the site was considerably affected by the transports of pollutants from the polluted urban area, including urban superimposed emission from the Beijing city center, Baoding, Shijiazhuang Tianjin, and Langfang.

3.2 Evaluation of HCHO during the APEC

The MAX-DOAS results in the period of October 26, 2014 to November 20, 2014 are used to evaluate the HCHO values during the APEC. The period is splited into three episodes. The first episode was defined as the period of APEC (from November 1, 2014 to November 12, 2014), wherein strict air quality policies were implemented at a regional scale. The

second and third episodes were defined as the "pre-APEC" from October 26, 2014 to October 31, 2014 and the "post-parade" from November 13, 2014 to November 20, 2014.

Fig. 9 presents the varying series of the daily mean values of HCHO VCDs during the APEC in three episodes. The result shows a "fluctuating effect" with the HCHO VCDs increasing abruptly in several days and dropping sharply for a few days during the APEC summit. This phenomenon is also observed in NO_2 VCD observations in Beijing urban area (Liu et al., 2016). The average HCHO VCDs are 9.65×10^{15}, 5.99×10^{15}, and 8.65×10^{15} molec cm^{-2} before, during, and after the APEC, respectively, A noticeable decreasing during the APEC by 37.95%, and 30.75% is found compared with before and after the APEC. The reduction could be attributed to the control measurements during the APEC. However the systematic difference of wind fields between the three episodes could also play a role considering the effects of transports of pollutants discussed in Sect. 3.1. The wind rose for wind speed at the three episodes is shown in **Fig. 10**. The prevailing wind direction of the three episodes is from northwest. The frequency of northwest winds in the APEC period is more than in the pre-APEC and post-APEC periods. And the wind speed in the APEC period is higher. Under the prevailing northwest wind, transports of pollutants from the polluted south area to the observed area are much fewer than those under the southerly winds. Therefore, the prevailing northwest wind fields may also contribute to the low HCHO during APEC.

Although two peak values (November 4, 2014 and November 7, 2014) were observed during APEC due to the transport, the peak values of HCHO decreasing about 25.75% and 18.3% compared to the peak values in the pre-APEC and post-APEC periods. It implies that the control measures have a certain effect on reducing the concentration of HCHO. It is consistent with that the implementation of control measures during the APEC summit reduced the concentrations of NO_2 and aerosols (Liu et al., 2016; Zhang et al., 2017). Both Chinese stringent control policy and prevailing northwest wind fields lead to the significant reduction of HCHO in Beijing during APEC.

3.3 Sources of HCHO

The hourly averaged HCHO VCDs on three episodes were analyzed to characterize the diurnal variation (**Fig. 11**). The hourly averaged HCHO VCDs exhibited evident daily variation. High values appear at early afternoon and low values appear in the morning. Atmospheric photochemical reaction is related to the intensity of solar radiation. The atmospheric

photochemistry reaction is generally active when the intensity of solar radiation is strong. Therefore, HCHO productivity of the secondary sources is high (Anderson et al., 1996). The peaks of diurnal variation generally emerge at 14:00, which is likely related to the diurnal variations of photochemical reaction rates. Other small peaks appear in the evening for another period of busy traffic (16:00–18:00 LT), which might be caused by primary pollution sources, e.g. vehicle exhausts. Thus, the diurnal variation of HCHO was similar to the secondary sources patterns during all the three episodes. The absolute HCHO values during the APEC period are obviously lower than those in the pre-APEC and post-APEC periods. The averaged HCHO during evening rush hours after APEC was higher than that before APEC. This finding is an interesting phenomenon, which may be related to some measures taken before the APEC.

Determining the pollution sources is crucial to controlling air pollution. Three time intervals were used for analysis to determine the main HCHO sources. The first interval was defined as noontime from 11:00–14:00 with strong photochemical reactions. And the second and third intervals were defined as morning rush hour from 7:00–9:00 and evening rush hour from 16:00–18:00. To further determine whether the pollution sources of HCHO at UCAS are primary or secondary formations from other VOCs, the correlations of HCHO with the primary pollutant NO_2 or secondary pollutant O_3 are analyzed (Anderson et al, 1996; Possanzini et al., 2002). Surface O_3 data were obtained from in situ measurements and the troposphere NO_2 VCD were retrieved from the MAX-DOAS measurements. The linear correlation of noon time averaged HCHO VCD with O_3 from 11:00–14:00 and rush hour average HCHO VCD with NO_2 VCD from 7:00–9:00 and 16:00–18:00 are shown in **Fig.12**. Direct analysis of the data shows that noon time average HCHO has a higher correlation coefficient with O_3, with a correlation coefficient of 0.934. By contrast, poor correlation with a correlation coefficient of 0.232 is found between HCHO and NO_2 during the rush hours. This result indicates that secondary photo-oxidation formation of HCHO from other VOCs should be the dominant source in UCAS.

3.4. Comparisons with model data

HCHO VCDs retrieved from MAX-DOAS measurements are compared with those from CAMS model data from the period of October 1, 2014 to December 31, 2014 **(Fig. 13)**. The average value of the data from MAX-DOAS in the period of 7:30 to 8:30 LT was selected for comparison with the CAMS data at 0:00 UTC (8:00 LT). And the data from MAX-DOAS in the

period 13:30 to 14:30 LT was averaged for comparisons with the CAMS data at 6:00 UTC (14:00 LT) (**Fig. 13a and 13c**). The CAMS model results with different grids are shown in **Fig. 13** and their differences are negligible. The CAMS model underestimates HCHO VCDs by 1.56–2.02 $\times 10^{15}$ molec cm^{-2} and 1.27–2.12 $\times 10^{15}$ molec cm^{-2} compared to MAX-DOAS measurements on average at 8:00 LT and 14:00 LT, respectively. The correlation coefficients and linear regressions between the MAX-DOAS and the model results are shown in **Fig. 14**. The correlation coefficient R is more than 0.827 and 0.886 at 8:00 LT and 14:00 LT, respectively. Comparison results in **Fig. 13 and 14** show that the CAMS model and MAX-DOAS results are generally consistent, especially the peak values are well consistently captured by both data sets, but the low values are systematically underestimated by the CAMS model. Because the peak values are mostly related to the transports of pollutants from the southern area, the well consistency of the peak values between MAX-DOAS and CAMS model implies the CAMS model can well simulate the transports of pollutants. In addition, in the CAMS model, only gas phase chemical reactions are considered for HCHO as described in section 2.5. Therefore the well consistency of HCHO values between MAX-DOAS measurements and CAMS simulations indicate that the heterogeneous reactions could not dominate the secondary formation of HCHO from other VOCs. The underestimations of low HCHO values by the CAMS model compared to MAX-DOAS measurements could be attributed to worse constraint of local emissions in the model near the UCAS measurement station. There is a nearby China National Highway 111 that runs along north to south. Because the UCAS is in the suburban area of Beijing, the vehicle emission could dominate HCHO amount under the situation with weak transports of pollutants from the polluted southern area. In general CAMS model can well capture the distinct day-to-day variations of HCHO. In addition day-to-day variations of HCHO could be attributed to variations of transports of pollutants, secondary formation rate of HCHO, and local primary emissions. Because a constant primary emission rate is assumed in the CAMS model simulations, meanwhile fluctuation amplitudes of solar radiance and temperature, which impact the secondary formation rate of HCHO, are much smaller than the day-to-day variations of HCHO, therefore transports of pollutants could be the dominant factor of the captured distinct day-to-day variations of HCHO

Underestimation of HCHO by the CAMS model becomes significant after December 1, 2014. The phenomenon could be related to the decreasing of the temperature after December 1, 2014. Time series of coincident hourly averaged meteorological parameters measured at supersite from October 28 to December 31, 2014 at 8:00 and 14:00 LT are shown in

Fig.13b and d, respectively. The temperature is an important parameter to impact the production rate of secondary HCHO. When the temperature decreases, the generation yield of the secondary photochemical reaction to produce HCHO decreases, resulting in low concentration of HCHO. The temperature dramatically dropped after December 1, 2014, which could cause the low production rate of HCHO. The secondary sources of HCHO can be better simulated than the local primary sources in the model (Stavrakou et al., 2014; Anderson et al., 2015; Kwon et al., 2017). In another word, the CAMS model could underestimate the local primary emission of HCHO, but the MAX-DOAS measurements can well obtain the HCHO both from the local primary emission and secondary generation. Thus, when the secondary source of HCHO is reduced, namely the primary HCHO is dominant, the difference between the MAX-DOAS observation and CAMS model is obvious.

The consistency of $R_{MAX\text{-}DOAS}$ and R_{Model} can be used to characterize the ability of model to simulate diurnal variation of HCHO. The $R_{MAX\text{-}DOAS}$ and R_{Model} are calculated as following Eq.(3) and Eq.(4):

$$R_{MAX\text{-}DOAS} = \frac{HCHO\ VCD_{MAX\text{-}DOAS\ at\ 8:00\ LT}}{HCHO\ VCD_{MAX\text{-}DOAS\ at\ 14:00\ LT}} \quad (3)$$

$$R_{model} = \frac{HCHO\ VCD_{model\ at\ 8:00\ LT}}{HCHO\ VCD_{model\ at\ 14:00\ LT}} \quad (4)$$

The scatter plots and linear regressions of daily $R_{MAX\text{-}DOAS}$ and R_{Model} are given in **Fig. 15**. Although large scatters are found, but most of the dots are around 1:1 line. Therefore the model can reasonably simulate the systematic diurnal variation of HCHO.

Clouds could impact the MAX-DOAS measurements. The effects could impact the comparisons between MAX-DOAS and CAMS model. In order to test the effect, we compare MAX-DOAS and CAMS model HCHO results under different effective cloud fractions (eCF) from the ECMWF (**Table S1 in the Supplement**) (**Fig. S1 and S2 in the Supplement).** The consistencies between the two data have slight variety as the cloud fractions increases. This outcome shows that clouds have little effect on the comparisons of MAX-DOAS and model, which is consistent to the result in Wang et al., 2017b.

4 Conclusions

We studied the tropospheric HCHO VCDs at the UCAS site in Huairou District, Beijing during the APEC summit based on the MAX-DOAS measurement from October 1, 2014 to December 31, 2014.

The UCAS site was affected by transport of pollutants from south. Two peak values on November 4 and November 7, 2014 during the APEC summit was caused by a change of wind direction to the south and an increase of wind speed of > 2.0 m s^{-1} when the polluted air masses from the south were transported to the UCAS site. Marked wind speed and direction dependence of HCHO VCDs were identified. Wind direction dependencies indicated that the HCHO values in the area around UCAS are considerably affected by the transports of pollutants from the south, including southwest and southeast where heavy polluted cities are located, such as Tangshan, Shijiazhuang, and Tianjin. By contrast, winds from north and northeast contributes to the dispersion of HCHO.

The impact of control measures on HCHO is evaluated using approximately one month MAX-DOAS data from October 26 to November 20, 2014, which was defined in three episodes. The first episode is the period of APEC (from November 1-12); the second and third episodes are the "pre-APEC" period from October 26, 2014 to October 31, 2014 and the "post-parade" from November 13, 2014 to November 20, 2014. During the period of APEC conference, the averaged HCHO is 9.65×10^{15} molec cm^{-2}, which is 37.95% and 30.75% lower than that during the pre-APEC and post-APEC period, respectively. Prevailing northwest wind fields and strict control measures working together lead to the relative low HCHO values during the APEC.

The daily variation of HCHO VCDs at the UCAS site indicates that the values at noon and evening rush hour are higher than those in the morning. And the peak values appear around noon. In addition, a good correlation coefficient of 0.87 between HCHO and O_3 is found around noon time. This finding indicates that the secondary sources of HCHO through photochemical reactions dominate in the area around UCAS.

The time series of HCHO VCDs retrieved by MAX-DOAS and CAMS model are consistent from October 1, 2014 to December 31, 2014. The CAMS model underestimates HCHO VCD by about 1.27–2.12 $\times 10^{15}$ molec cm^{-2} compared to MAX-DOAS measurements on average. The CAMS model can well simulate the effects of transports and the secondary source of HCHO, but underestimate the local primary source, which is more pronounced under the situation with a low temperature when the production rate of secondary HCHO is relatively low. Generally consistent ratios of HCHO VCDs at around 8:00 LT and 14:00 are found for the CAMS model simulations and MAX-DOAS measurements. It indicates that the CAMS model can reasonably simulate the systematic diurnal variation of HCHO.

Acknowledgment

We thank the Belgian Institute for Space Aeronomy (BIRA–IASB) in Brussels, Belgium for the freely accessible Windoas software and the European Meteorology Center for providing free medium-range weather forecasts for CAMS real-time products of HCHO. We also thank the University of Chinese Academy of Sciences and Peking University for their support and assistance in the observation and supply of essential data. This study was supported by the National Natural Science Foundation of China (Grant Nos.: 41530644, 41405033, and 41605013).

Reference

Anders P.: European Centre for Medium-Range Weather Forecasting, 2015, http://apps.ecmwf.int/datasets/data/cams-nrealtime/levtype=sfc/

Anderson, L.G., Lanning, J.A., Barrell, R., Miyagishima, J., Jones, R.H., Wolfe, P.: Sources and sinks of formaldehyde and acetaldehyde: An analysis of Denver's ambient concentration data, Atmos. Environ., 30, 2113-2123, doi:10.1016/1352-2310(95)00175-1, 1996.

Bobrowski, N., Hã Nninger, G., Galle, B., Platt, U.: Detection of bromine monoxide in a volcanic plume, Nature, 423, 273-276, doi:10.1038/nature01625, 2003.

Borovski, A.N., Dzhola, A.V., Elokhov, A.S., Grechko, E.I., Kanaya, Y., Postylyakov, O.V.: First measurements of formaldehyde integral content in the atmosphere using MAX-DOAS in the Moscow region, Int. J. Remote. Sens., 35, 5609-5627, 2014.

Brinksma, E.J., Pinardi, G., Volten, H., Braak, R., Richter, A., Schönhardt, A., Roozendael, M. V., Fayt, C.,Hermans, C., Dirksen R. J., Vlemmix, T., Berkhout, A. J. C., Swart, D. P. J., Oetjen, H., Wittrock, F., Wagner, T., Ibrahim, O. W., Leeuw, G. D., Moerman, M., Curier, R. L., Celarier, E. A., Cede, A., Knap, W. H., Veefkind, J. P., Eskes, H. J., Allaart, M., Rothe, R., Piters, A. J. M., Levelt, P. F.: The 2005 and 2006 DANDELIONS BO2 and aerosol intercomparison campaigns. Journal of Geophysical Research, accepted for publication,113, D16S46, doi:10.1029/2007JD008808, 2008.

Chance, K., Palmer, P. I., Spurr, R. J., Martin, R. V., Kurosu, T. P., and Jacob D. J.: Satellite observations of formaldehyde over North America from GOME, Geophys. Res. Lett., 27, 3461–3464, 2000.

Chance, K.V., Spurr, R.J.. Ring effect studies: Rayleigh scattering, including molecular parameters for rotational Raman scattering, and the Fraunhofer spectrum. Appl. Optics. 36(21), 5224-5230, doi:10.1364/AO.36.005224, 1997.

Cheng, N.L., Li, Y.T., Zhang, D.W., Chen, T., Li, L.J., Li, J., Jiang, L.: Improvement of Air Quality During APEC in Beijing in 2014, Environmental Science, 37, 66-73, DIO:10.13227/j.hjkx.2016.01.001, 2016.

Cheung, R., Colosimo, S.F., Pikelnaya, O., Stutz, J.: MAX-DOAS Measurements of NO2 and HCHO in Los Angeles from an Elevated Mountain Site at Mt. Wilson, California, Sensors-Basel, 14, 2449-2467, 2014.

Clémer, K., Roozendael, M.V., Fayt, C., Hendrick, F.: Multiple wavelength retrieval of tropospheric aerosol optical properties from MAXDOAS measurements in Beijing, Atmos. Meas. Tech., 3, 863-878, doi:10.5194/amt-3-863-2010, 2010.

De Smedt, I., Van Roozendael, M., Stavrakou, T., Müller, J.-F., Lerot, C., Theys, N., Valks, P., Hao, N., and van der A, R.: Improved retrieval of global tropospheric formaldehyde columns from GOME-2/MetOp-A addressing noise reduction and instrumental degradation issues, Atmos. Meas. Tech., 5, 2933–2949, doi:10.5194/amt-5-2933-2012, 2012.

De Smedt, I., Stavrakou, T., Hendrick, F., Danckaert, T., Vlemmix, T., Pinardi, G., Theys, N., Lerot, C., Gielen, C., Vigouroux, C., Hermans, C., Fayt, C., Veefkind, P., Müller, J.-F., and Van Roozendael, M.: Diurnal, seasonal and long-term variations of global formaldehyde columns inferred from combined OMI and GOME-2 observations, Atmos. Chem. Phys., 15, 12519-12545, doi:10.5194/acp-15-12519-2015, 2015.

Erle, F., Pfeilsticker, K., Platt, U.: On the influence of tropospheric clouds on zenith - scattered - light measurements of stratospheric species, Geophys. Eophys. Res. Lett., 22(20), 2725-2728, doi:10.1029/95GL02789, 2013.

Fan, S.B., Tian, L.D., Zhang, D.X., Guo, J.J.: Evaluation on the Effectiveness of Vehicle Exhaust Emission Control Measures During the APEC Conference in Beijing, Environmental Science, 37, 74-81, doi:10.13227/j.hjkx.2016.01.001, 2016.

Fish, D.J., Jones, R.L.: Rotational Raman scattering and the ring effect in zenith - sky spectra, Geophys. Res. Lett., 22, 811-814, doi:10.1029/95GL00392, 2013.

Fleischmann, O.C., Hartmann, M.: New ultraviolet absorption cross-sections of BrO at atmospheric temperatures measured

by time-windowing Fourier transform spectroscopy, J. Photochem. Photobiol. A chem., 168, 117-132, doi:10.1016/j.jphotochem.2004.03.026, 2004.

Flemming, J., Huijnen, V., Arteta, J., Bechtold, P., Beljaars, A., Blechschmidt, A.M., Diamantakis, M., Engelen, R.J., Gaudel, A., Antje Inness, A., Jones, L., Katragkou, E., Peuch, V.H., Richter, A., Schultz, M.G., Stein, O.,Tsikerdekis, A.: Tropospheric Chemistry in theIntegrated Forecasting System of ECMWF, ECMWF Technical Memoranda, 1-52, 2014.

Franco, B., Hendrick, F., Van Roozendael, M., Müller, J.F., Stavrakou, T., Marais, E.A., Bovy, B., Bader, W., Fayt, C., Hermans, C.: Retrievals of formaldehyde from ground-based FTIR and MAX-DOAS observations at the Jungfraujoch station and comparisons with GEOS-Chem and IMAGES model simulations, Atmos. Meas. Tech., 8, 1733-1756, doi:10.5194/amt-8-1733-2015, 2015.

Halfacre, J.W., Knepp, T.N., Stephens, C.R., Pratt, K.A., Shepson, P., Simpson, W.R., et al.: Temporal and spatial characteristics of ozone depletion events, Atmos. Chem. Phys., 14: 4875–4894, doi:10.5194/acp-14-4875-2014, 2014.

Fried, A., Cantrell, C., Olson, J., Crawford, J. H.: Detailed comparisons of airborne formaldehyde measurements with box models during the 2006 INTEX-B and MILAGRO campaigns: potential evidence for significant impacts of unmeasured and multi-generation volatile organic carbon compounds, Atmos. Chem. Phys., 11, 9887-9957, doi:10.5194/acp-11-11867-2011, 2011.

Hendrick, F., Müller, J.-F., Clémer, K., Wang, P., De Mazière, M., Fayt, C., Gielen, C., Hermans, C., Ma, J. Z., Pinardi, G., Stavrakou, T., Vlemmix, T., and Van Roozendael, M.: Four years of ground-based MAX-DOAS observations of HONO and NO2 in the Beijing area, Atmos. Chem. Phys., 14, 765–781, doi:10.5194/acp-14-765-2014, 2014.

Hermans, C., Vandaele, A.C., Fally, S., Carleer, M., Colin, R., Coquart, B., Jenouvrier, A., Merienne, M.F.: Absorption Cross-section of the Collision-Induced Bands of Oxygen from the UV to the NIR, Springer Netherlands, 193-202, 2003.

Hönninger, G., Friedeburg, C. V., and Platt, U.: Multi axis differential optical absorption spectroscopy (MAX-DOAS), Atmos. Chem. Phys., 4, 231-254, doi:10.5194/acp-4-231-2004, 2004.

Kraus, S.: DOASIS-A Framework Design for DOAS. PhD Thesis, University of Heidelberg, Heidelberg, Germany, 2006.

Hönninger, G., Platt, U.: Observations of BrO and its vertical distribution during surface ozone depletion at Alert, Atmos. Environ., 36, 2481-2489, doi:10.1016/S1352-2310(02)00104-8, 2002.

Kwon, H.A., Park, R., Nowlan, C., González Abad, G.K., Janz, S.: Formaldehyde (HCHO) column measurements from airborne instruments: Comparison with airborne in-situ measurements, model, and satellites, 19th EGU General Assembly, EGU2017, proceedings from the conference held 23-28 April, 2017 in Vienna, Austria., p.11084 , 2017.

Lee, H., Ryu, J., Irie, H., Jang, S.H., Park, J., Choi, W., Hong, H.: Investigations of the Diurnal Variation of Vertical HCHO Profiles Based on MAX-DOAS Measurements in Beijing: Comparisons with OMI Vertical Column Data, Atmos., 6, 1816-1832, doi:10.3390/atmos6111816, 2015.

Li, X., Brauers, T., Hofzumahaus, A., Lu, K., Li, Y.P., Shao, M., Wagner, T., Wahner, A.: MAX-DOAS measurements of NO2, HCHO and CHOCHO at a rural site in Southern China, Atmos. Chem. Phys, 13, 2133-2151, doi:10.5194/acp-13-2133-2013, 2013.

Liu, H.R., Liu, C., Xie, Z.Q., Li, Y., Huang, X., Wang, S.S., Xu, J., Xie, P.H.: A paradox for air pollution controlling in China revealed by "APEC Blue" and "Parade Blue". Sci. Rep. UK 6, 34408, doi:10.1038/srep34408, 2016.

Liu, J. G., Xie, P. H., Wang, Y. S., Wang, Z. F., He, H., Liu, W. Q.: Haze Observation and Control Measure Evaluation in Jing-Jin-Ji (Beijing, Tianjin, Hebei) Area during the Period of the Asia-Pacific Economic Cooperation (APEC) Meeting, S & T and society 30, 368-377, doi:10.16418/j.issn.1000-3045.2015.03.011, 2015.

Meller, R., Moortgat, G.K.: Temperature dependence of the absorption cross sections of formaldehyde between 223 and 323 K in the wavelength range 225–375 nm, J. Geophys. Res. Atmos., 105, 7089-7101, doi:10.1029/1999JD901074, 2000.

Nilsson, J. A., Zheng, X., Sundqvist, K., Liu, Y., Atzori, L., Elfwing, A., Arvidson, K., Grafström, R.C.: Toxicity of Formaldehyde to Human Oral Fibroblasts and Epithelial Cells: Influences of Culture Conditions and Role of Thiol Status, J Dent. Res., 77(11), 1896-1903, 1998.

Nninger, G.H., Friedeburg, C.V., Platt, U.: Multi axis differential optical absorption spectroscopy (MAX-DOAS). Atmos. Chem. Phys. 4, 231-254, doi:10.5194/acp-4-231-2004, 2004.

Palmer, P.I., Abbot, D.S., Fu, T.M., Jacob, D.J., Chance, K., Kurosu, T.P., Guenther, A., Wiedinmyer, C., Stanton, J.C., Pilling, M.J.: Quantifying the seasonal and interannual variability of North American isoprene emissions using satellite observations of the formaldehyde column, J. Geophys. Res. Atmos., 111, 2503-2511, doi:10.1029/2005JD006689, 2006.

Persson, A., Grazzini, F.: User guide to ECMWF forecast products, Meteorol Bull 3, Designed, edited and printed by

ECMWF, 2001.

Pinardi, G., Roozendael, M.V., Abuhassan, N., Adams, C., Cede, A., Clémer, K., Fayt, C., Frieß, U., Gil, M., Herman, J.: Intercomparison of MAXDOAS HCHO slant columns during the CINDI campaign, Atmos. Meas. Tech., 6, 219, 2012.

Pinardi, G., Van Roozendael, M., Abuhassan, N., Adams, C., Cede, A., Clémer, K., Fayt, C., Frieß, U., Gil, M., Herman, J., Hermans, C., Hendrick, F., Irie, H., Merlaud, A., Navarro Comas, M., Peters, E., Piters, A.J.M., Puentedura, O., Richter, A., Schönhardt, A., Shaiganfar, R., Spinei, E., Strong, K., Takashima, H., Vrekoussis, M., Wagner, T., Wittrock, F., Yilmaz, S.: MAX-DOAS formaldehyde slant column measurements during CINDI: intercomparison and analysis improvement, Atmos. Meas. Tech., 6, 167-185, doi:10.5194/amt-6-167-2013, 2013.

Possanzini, M., Palo, V.D., Cecinato, A.: Sources and photodecomposition of formaldehyde and acetaldehyde in Rome ambient air, Atmos. Environ., 36, 3195-3201, doi:10.1016/S1352-2310(02)00192-9, 2002.

Roozendael, M.V., Post, P., Hermans, C., Lambert, J.C., Fayt, C.. Retrieval of BrO and NO2 from UV-visible observations, Sounding the Troposphere from Space, Springer, Berlin, Heidelberg, 155-165, 2003.

Schreier, S.F., Richter, A., Wittrock, F., Burrows, J.P.: Estimates of free-tropospheric NO2 and HCHO mixing ratios derived from high-altitude mountain MAX-DOAS observations at midlatitudes and in the tropics, Atmos. Chem. Phys., 16, 2803-2817, doi:10.5194/acp-16-2803-2016, 2016.

Serdyuchenko, A., Gorshelev, V., Weber, M., Chehade, W., Burrows, J.P.: High spectral resolution ozone absorption cross-sections - Part 2: Temperature dependence, Atmos. Meas. Tech., 7, 625-636, doi.org/10.5194/amt-7-625-2014, 2013.

Sinreich, R., Friess, U., Wagner, T., Platt, U.: Multi axis differential optical absorption spectroscopy (MAX-DOAS) of gas and aerosol distributions, Faraday Discuss, 130, 153-164, doi:10.1039/B419274P, 2005.

Solberg, S., Dye, C., Walker, S.E., Simpson, D.: Long-term measurements and model calculations of formaldehyde at rural European monitoring sites, Atmos. Environ., 35, 195-207, doi:10.1016/S1352-2310(00)00256-9, 2001.

Starn, T.K., Shepson, P.B., Bertman, S.B., Riemer, D.D., Zika, R.G., Olszyna, K.: Nighttime isoprene chemistry at an urban-impacted forest site, J. Geophys. Res. Atmos., 103, 22437-22447, doi:10.1029/98JD01201, 1998.

Stavrakou, T., Müller, J.F., Smedt, I.D., Roozendael, M.V., Werf, G.R.V.D., Giglio, L., Guenther, A.: Global emissions of non-methane hydrocarbons deduced from SCIAMACHY formaldehyde columns through 2003-2006, Atmos. Chem. Phys., 9,

3663-3679, doi:10.5194/acp-9-3663-2009, 2009.

Stavrakou, T., Müller, J.F., Smedt, I.D., Roozendael, M.V., Werf, G.R.V.D., Giglio, L., Guenther, A.: Global emissions of non-methane hydrocarbons deduced from SCIAMACHY formaldehyde columns through 2003-2006, Atmos. Chem. Phys., 9, 3663-3679, doi:10.5194/acp-9-3663-2009, 2014.

Thalman, R., Volkamer, R.: Temperature dependent absorption cross-sections of O2-O2 collision pairs between 340 and 630 nm and at atmospherically relevant pressure, Phys. Chem. Chem. Phys., 15, 15371-15381, doi:10.1039/C3CP50968K, 2013.

Trebs, I., Meixner, F.X., Slanina, J., Otjes, R., Jongejan, P., Andreae, M.O.: MAX-DOAS measurements of atmospheric trace gases in Ny - lesund -Radiative transfer studies and their application, Atmos. Chem. Phys., 4, 6109-6145, doi:10.5194/acp-4-955-2004, 2004.

Vandaele, A.C., Hermans, C., Simon, P.C., Roozendael, M.V., Guilmot, J.M., Carleer, M., Colin, R.. Fourier transform measurement of NO2 absorption cross-section in the visible range at room temperature, J Atmos. Chem., 25(3), 289-305, 1996.

Vigouroux, C., Hendrick, F., Stavrakou, T., Dils, B.: Ground-based FTIR and MAX-DOAS observations of formaldehyde at Réunion Island and comparisons with satellite and model data, Atmos. Chem. Phys., 9, 9523-9544, doi:10.5194/acp-9-9523-2009, 2009.

Vrekoussis, M., Wittrock, F., Richter, A., Burrows, J.P.: GOME-2 observations of oxygenated VOCs: what can we learn from the ratio glyoxal to formaldehyde on a global scale? Atmos. Chem.. Phys. 10, 10145-10160, doi:10.5194/acp-10-10145-2010, 2010.

Wagner, T., Burrows, J.P., Deutschmann, T., Dix, B., Friedeburg, C.V., Frie, U., Hendrick, F., Heue, K.P., Irie, H., Iwabuchi, H.: Comparison of box-air-mass-factors and radiances for Multiple-Axis Differential Optical Absorption Spectroscopy (MAX-DOAS) geometries calculated from different UV/visible radiative transfer models, Atmos. Chem. Phys., 7, 1809-1833, doi:10.5194/acp-7-1809-2007, 2007.

Wagner, T., Deutschmann, T., Platt, U.: Determination of aerosol properties from MAX-DOAS observations of the Ring effect, Atmos. Meas. Tech., 2, 495-512, doi:10.5194/amt-2-495-2009, 2009.

Wagner, T., B. Dix, C. von Friedeburg, Frieß, U., Sanghavi, S., Sinreich, R. and Platt, U.: MAX-DOAS O_4 measurements: A

new technique to derive information on atmospheric aerosols—Principles and information content, J. Geophys. Res., 109, D22205, 2004.

Wagner, T., Beirle, S., Brauers, T., Deutschmann, T., Frieß, U., Hak, C., Halla, J. D., Heue, K. P., Junkermann, W., Li, X., Platt, U. and Pundt-Gruber, I.: Inversion of tropospheric profiles of aerosol extinction and HCHO and NO_2 mixing ratios from MAX-DOAS observations in Milano during the summer of 2003 and comparison with independent data sets, Atmos. Meas. Tech. Discuss, 4, 3891–3964, 2011.

Wang, G., Cheng, S., Wei, W., Yang, X., Wang, X., Jia, J., Lang, J., Lv, Z.: Characteristics and emission-reduction measures evaluation of PM2.5 during the two major events: APEC and Parade, Sci. Total Environ., 595, 81-92, 2017a.

Wang, Y., Beirle, S., Lampel, J., Koukouli, M., De Smedt, I., Theys, N., Li, A., Wu, D., Xie, P., Liu, C.: Validation of OMI, GOME-2A and GOME-2B tropospheric NO2, SO2 and HCHO products using MAX-DOAS observations from 2011 to 2014 in Wuxi, China: investigation of the effects of priori profiles and aerosols on the satellite products, Atmos. Chem. Phys., 17: 5007-5033, doi:10.5194/acp-17-5007-2017, 2017b.

Wang, Y., Lampel, J., Xie, P., Beirle, S., Li, A., Wu, D., Wagner, T.: Ground-based MAX-DOAS observations of tropospheric aerosols, NO2, SO2 and HCHO in Wuxi, China, from 2011 to 2014, Atmos. Chem. Phys., 17, 2189-2215, doi:10.5194/acp-17-2189-2017, 2017c.

Wang, Z.S., Li Y. T., Zhang, D.W., Chen, T., Sun F., Li, L.J.: Analysis on air quality in Beijing during the 2014 APEC conference, Acta Scientiae Circumstantiae, 36, 675-683, doi:10.13671/j.hjkxxb.2015.0495, 2016.

Zhang, J.S., Chen, Z.Y., Lu, Y.H. , Gui, H Q., Liu, J G., Liu, W.Q., Wang, J., Yu, T.Z., Cheng, Y., Chen, Y., Ge, B.Z., Fan, Y., Luo, X.S.: Characteristics of aerosol size distribution and vertical backscattering coefficient profile during 2014 APEC in Beijing, Atmos. Environ., 148, 30-41, 2017.

Zhang, Y.J., Pang, X.B., Mu, Y.J.: Contribution of isoprene emitted from vegetable to atmospheric formaldehyde in the ambient air of Beijing city, Environ. Sci., 30(4), 976-981, 2009.

Table

Atmos. Chem. Phys. Discuss., https://doi.org/10.5194/acp-2018-440
Manuscript under review for journal Atmos. Chem. Phys.
Discussion started: 4 June 2018

Atmospheric Chemistry and Physics Discussions

spectrometer		Azimuth	Elevation	Temperature	Location		Measuring time
Name	Maya	0 °	3 °, 5 °, 10 °, 15 °, 30 °, 90 °,	20 ℃	Site	Yanxi Lake campus of UCAS	6:30-18:30
Spectral range	290–420 nm				Longitude	116.67 °E	
FWHM	0.5 nm				Latitude	40.4 °N	

Table 1: Setting of MAX-DOAS.

Parameter	Data source	Fitting interval: nm 335–360 nm (HCHO) 338–360 nm (NO_2)
NO_2	Vandaele et al., (1996), 294 K	x
O_3	Serdyuchenko et al., (2013), 223 K, 243K	x
O_4	Thalman and Volkamer, (2013), 293 K	x
BrO	Fleischmann and Hartmann, (2004),223 K	x
HCHO	Meller and Moortgat, (2000), 293 K	x
Ring	Chance and Spurr, 1997	x
Polynomial degree		5

Table 2: Parameter settings used for spectral analysis using WINDOAS, where "x" indicates the cross section is used in the retrieval.

Figure

Atmos. Chem. Phys. Discuss., https://doi.org/10.5194/acp-2018-440
Manuscript under review for journal Atmos. Chem. Phys.
Discussion started: 4 June 2018

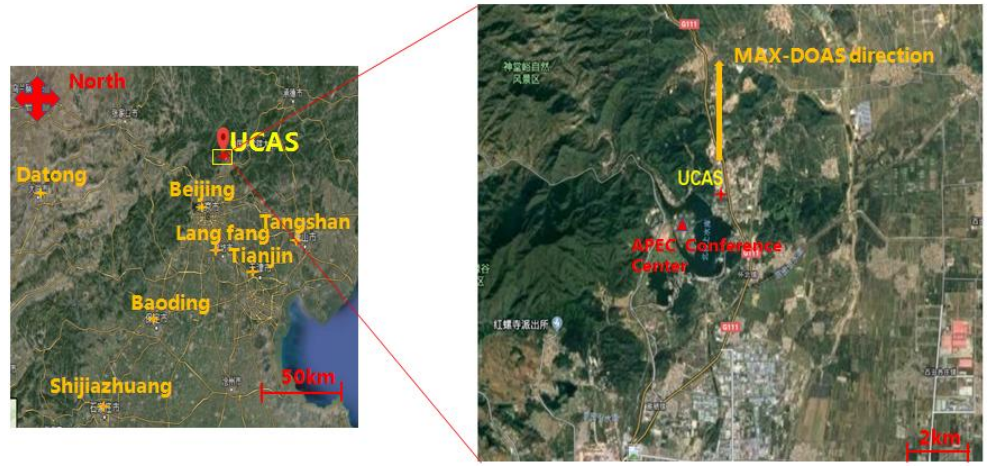

Figure 1: Supersite on the Yanqi Lake campus of UCAS.

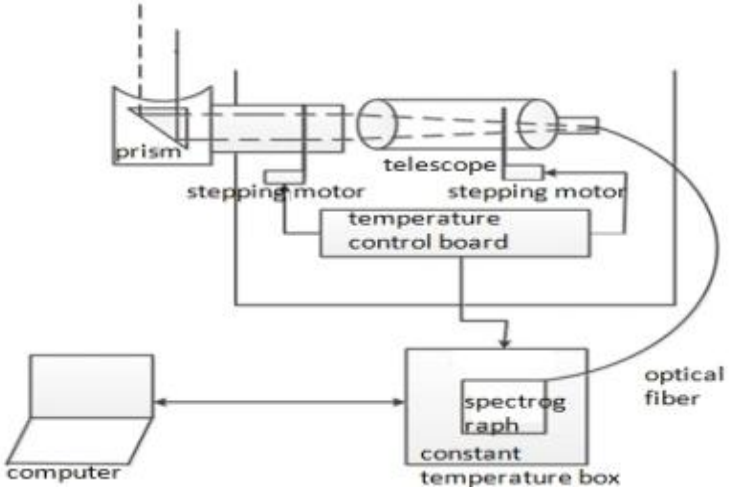

Figure 2: Experimental setup of MAX-DOAS.

Atmos. Chem. Phys. Discuss., https://doi.org/10.5194/acp-2018-440
Manuscript under review for journal Atmos. Chem. Phys.
Discussion started: 4 June 2018

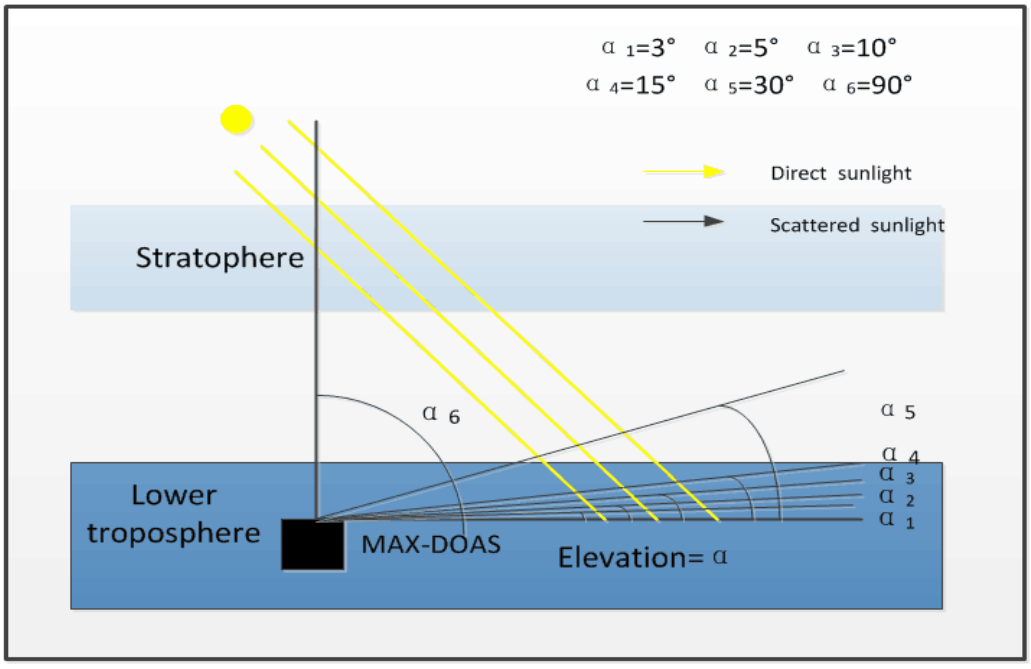

Figure 3: Observation geometry of MAX-DOAS.

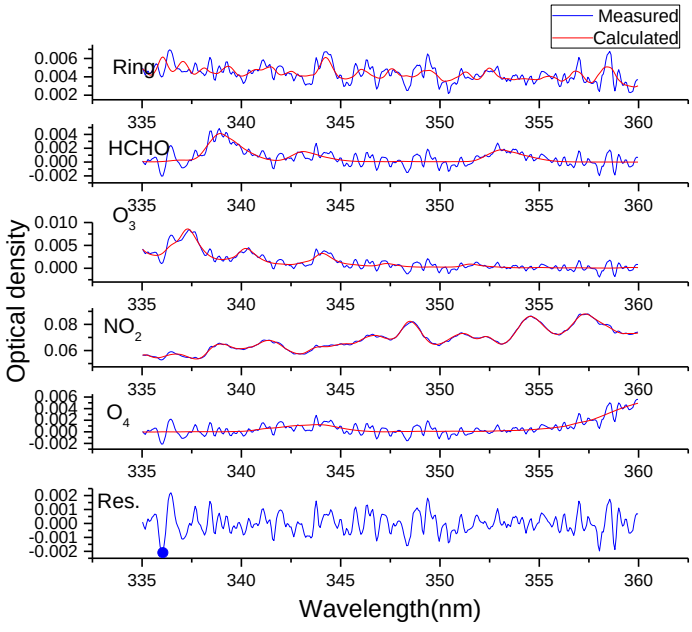

Figure 4: Example of a DOAS fit of a spectrum to retrieve the slant column densities of HCHO; the red and blue curves indicate the retrieved and the measured absorption structures, respectively.

Atmos. Chem. Phys. Discuss., https://doi.org/10.5194/acp-2018-440
Manuscript under review for journal Atmos. Chem. Phys.
Discussion started: 4 June 2018

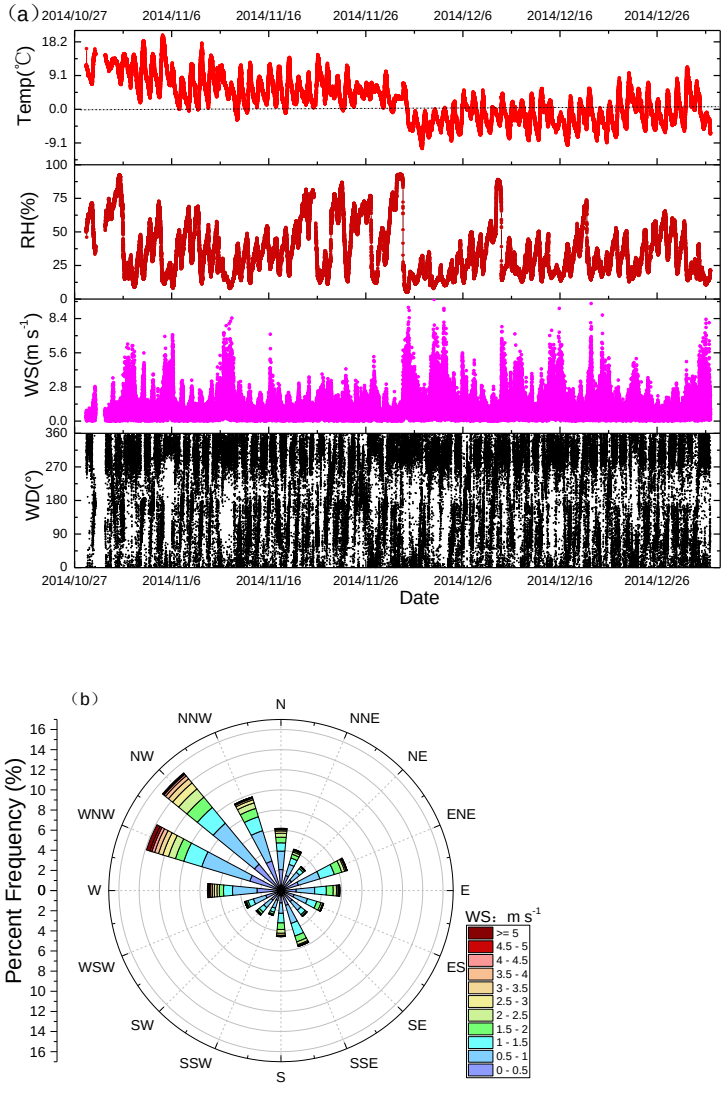

Figure 5: In the period of October 28, 2014 to December 31, 2014, (a)Time series of the meteorological parameters with a time resolution of 1 min containing ambient temperature, relative humidity (RH), the wind speed (WS) and direction (WD). (b) Wind rose.

Atmos. Chem. Phys. Discuss., https://doi.org/10.5194/acp-2018-440
Manuscript under review for journal Atmos. Chem. Phys.
Discussion started: 4 June 2018

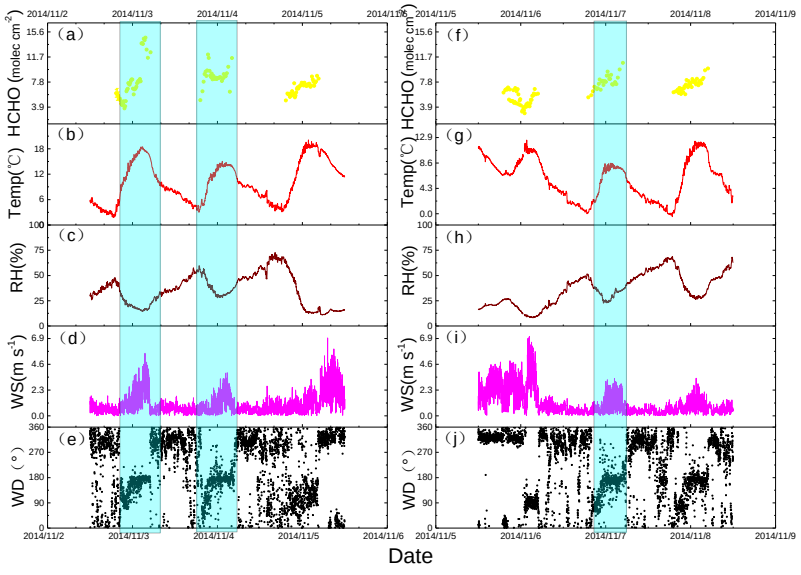

Figure 6: Time series of HCHO VCDs (molec cm^{-2}) and meteorological parameters (ambient temperature(℃), relative humidity (%), wind direction (°) and wind speed (m s^{-1})), measured at supersite in the two periods of November 3, 2014 to November 5, 2014 (Left column) and November 6 to November 8, 2014 (Right column).

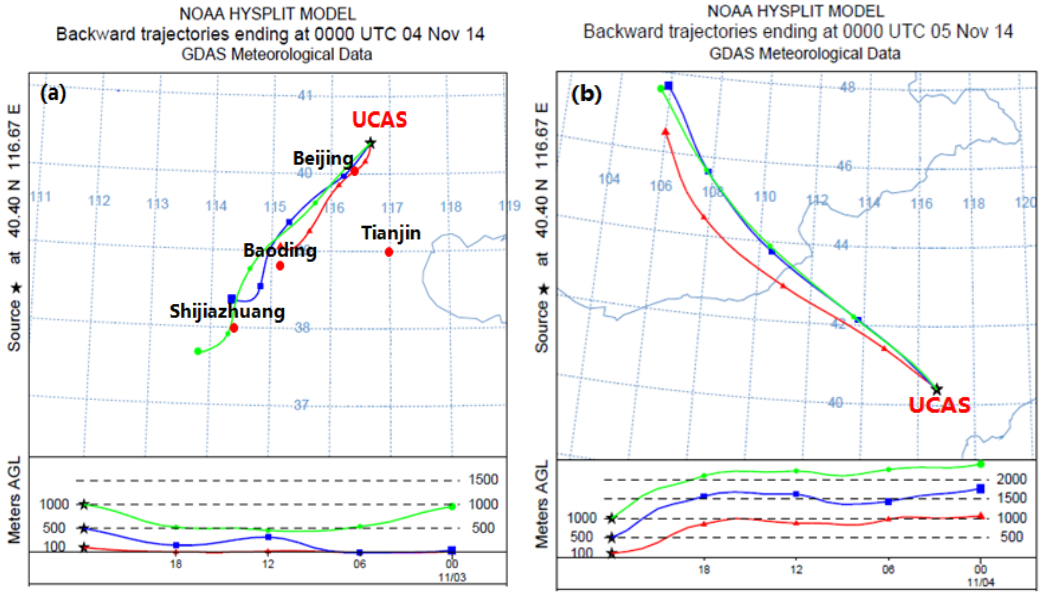

Atmos. Chem. Phys. Discuss., https://doi.org/10.5194/acp-2018-440
Manuscript under review for journal Atmos. Chem. Phys.
Discussion started: 4 June 2018

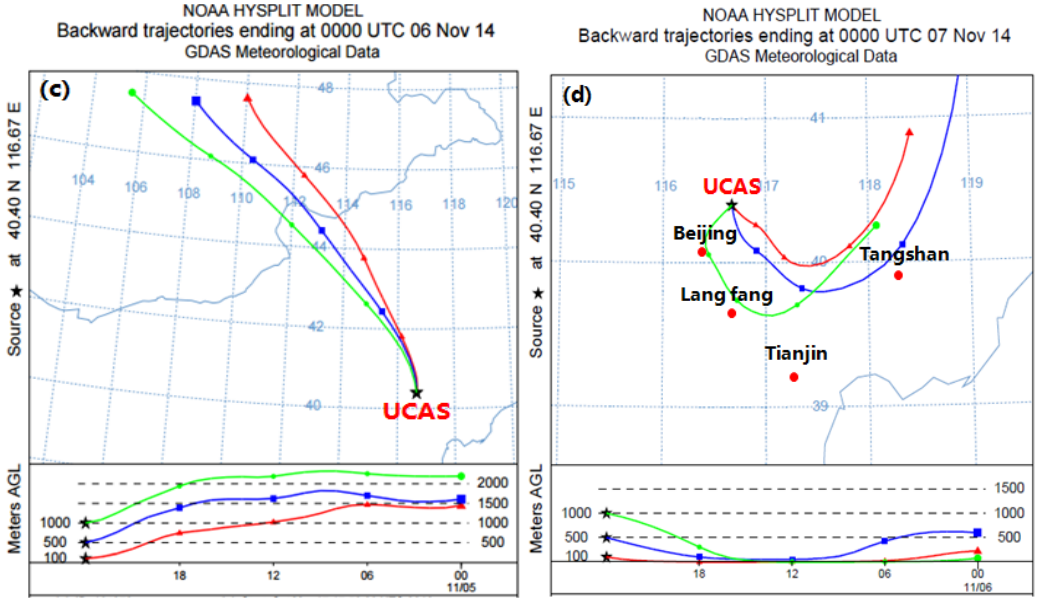

Figure 7: Backward trajectories determined (HYSPLIT) model at UCAS on November (a) 4, (b) 5, (c) 6 and (d) 7, 2014.

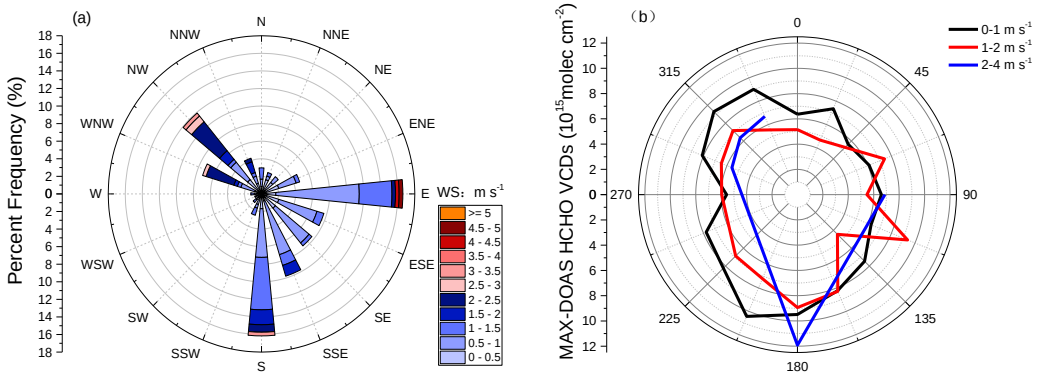

Figure 8: (a) Wind rose; (b) Dependence of HCHO VCD (10^{15} molec cm^{-2}) on wind directions for different wind speeds.

Atmos. Chem. Phys. Discuss., https://doi.org/10.5194/acp-2018-440
Manuscript under review for journal Atmos. Chem. Phys.
Discussion started: 4 June 2018

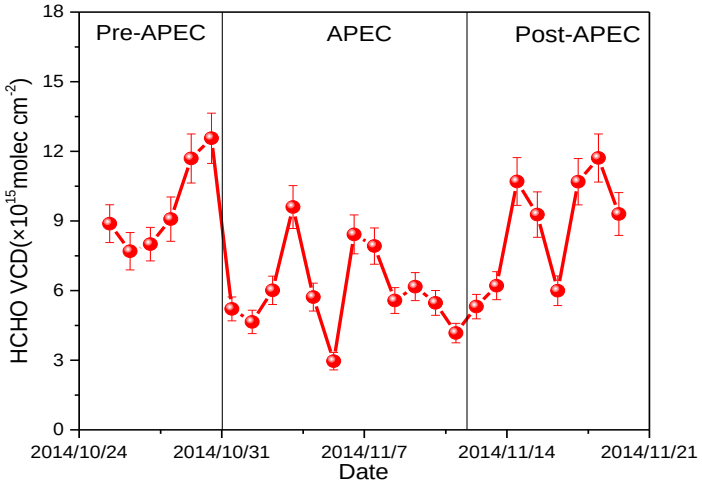

Figure 9: Daily averaged values of HCHO VCDs from October 26, 2014 to November 20, 2014. Error bars denote retrieval error.

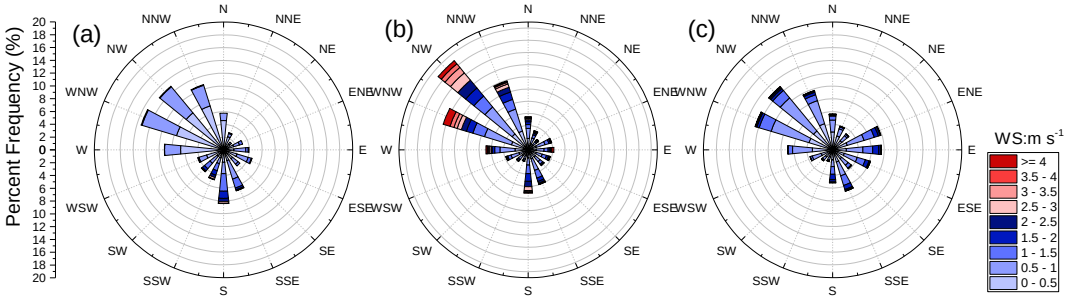

Figure 10: Wind roses in (a) the "pre-APEC" , (b) the APEC and (c) the "post-parade" periods.

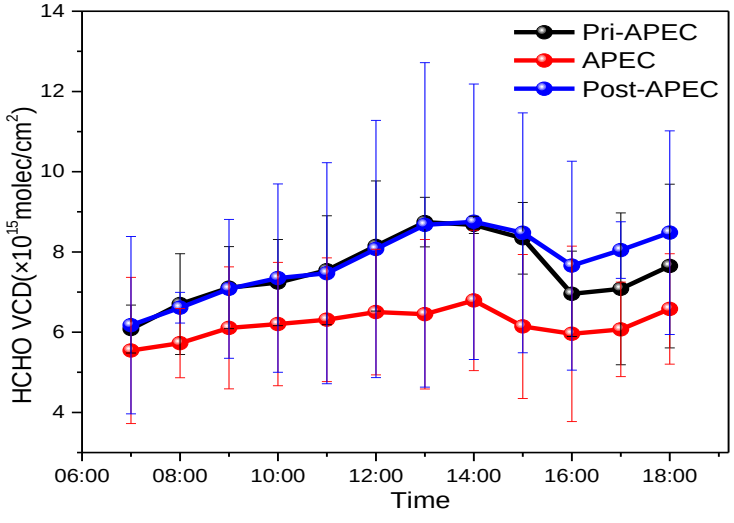

Atmos. Chem. Phys. Discuss., https://doi.org/10.5194/acp-2018-440
Manuscript under review for journal Atmos. Chem. Phys.
Discussion started: 4 June 2018

Atmospheric Chemistry and Physics Discussions

Figure 11: Averaged diurnal variation of HCHO VCDs measured by MAX-DOAS on three episodes around APEC. Error bars denote the one sigma standard deviations around the mean analysis values.

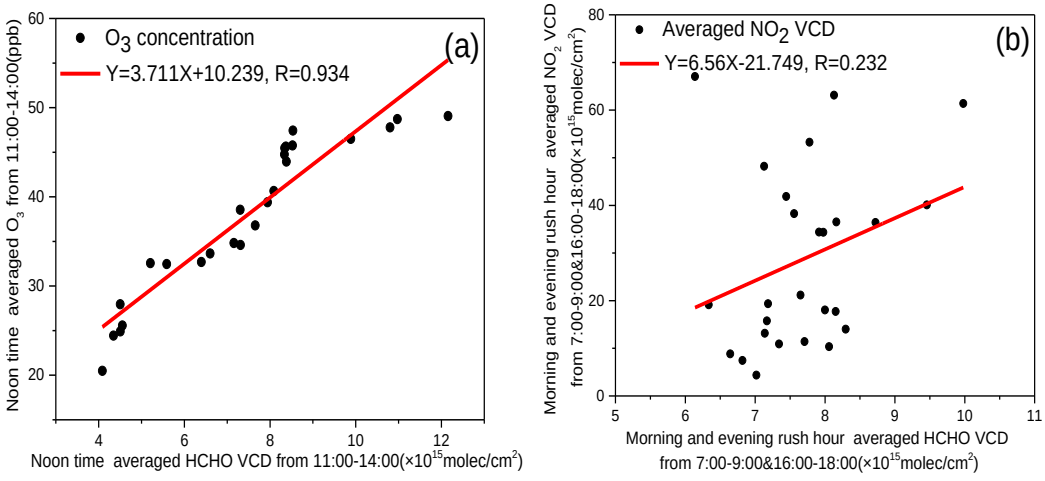

Figure 12: Scatter plots and linear regressions (a) of noon-time average HCHO VCD measured by MAX-DOAS against O_3 VMRs measured by stationary Ozone monitoring instrument, and (b) rush-hour average HCHO VCD against NO_2 VCD measured by MAX-DOAS in the period of October 26, 2014 to November 20, 2014.

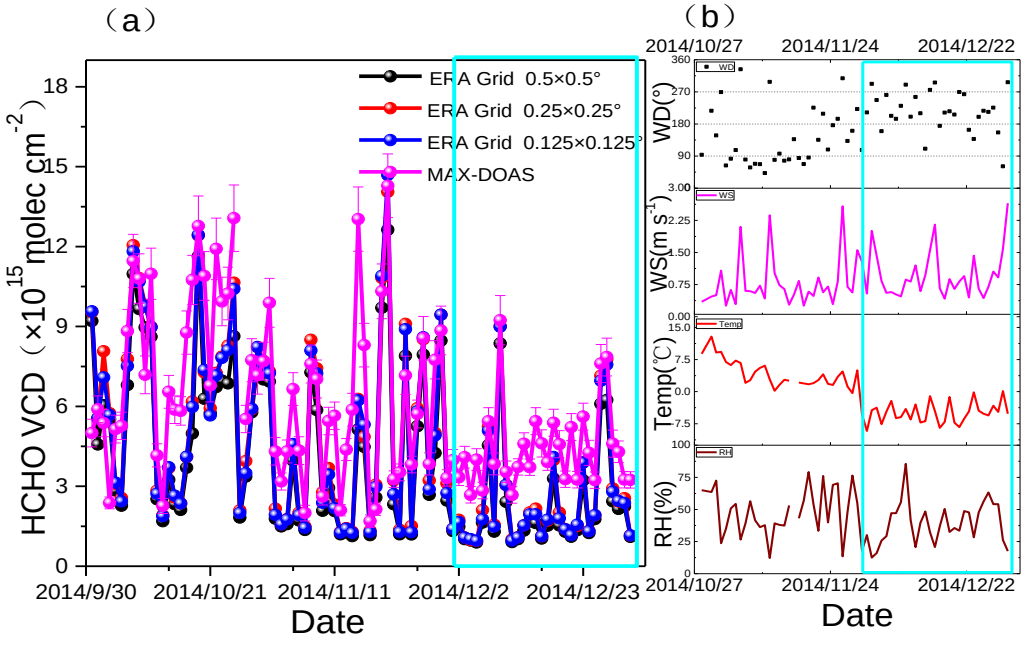

Atmos. Chem. Phys. Discuss., https://doi.org/10.5194/acp-2018-440
Manuscript under review for journal Atmos. Chem. Phys.
Discussion started: 4 June 2018

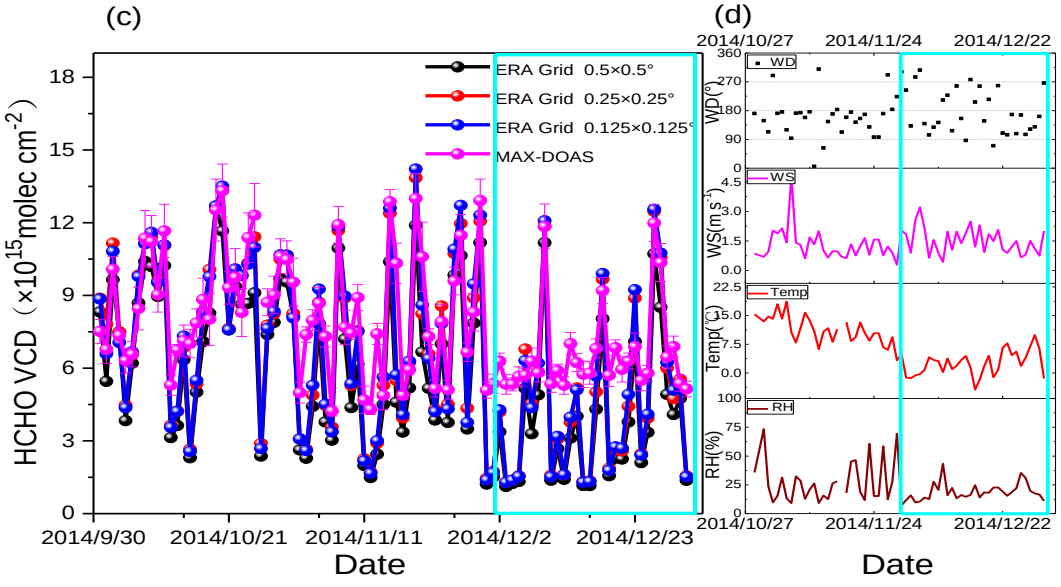

Figure 13: Hourly averaged HCHO VCDs derived from coincident CAMS model (grid of 0.125°× 0.125°, 0.25°× 0.25°, and 0. 5°× 0. 5°) and MAX-DOAS observations at 8:00 (a) and 14:00 LT (c) from October to December 2014. Error bars denote retrieval error. Time series of coincident hourly averaged meteorological parameters measured at supersite at 8:00 (b) and 14:00 LT (d) from October 28 to December 31, 2014.

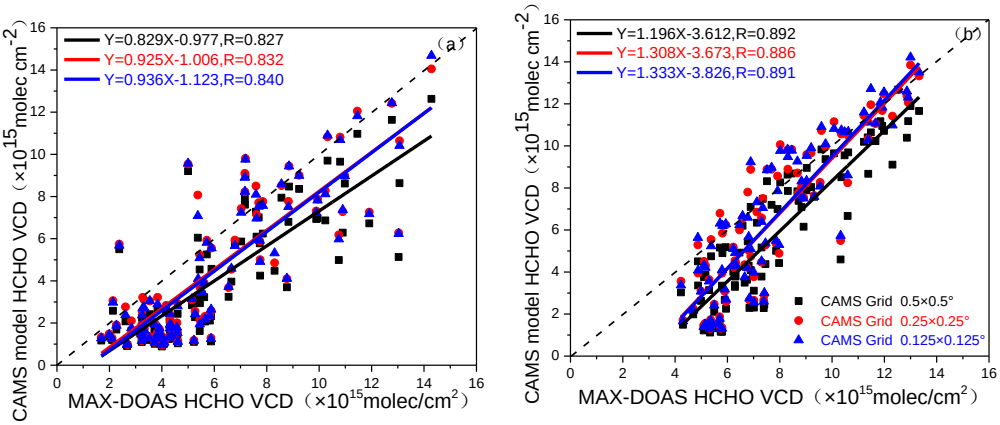

Figure 14: Correlation between HCHO VCDs retrieved from the MAX-DOAS measurements and those obtained from the CAMS model at 8:00 LT (a) and 14:00 LT (b) from October to December 2014 in different grids.

Atmos. Chem. Phys. Discuss., https://doi.org/10.5194/acp-2018-440
Manuscript under review for journal Atmos. Chem. Phys.
Discussion started: 4 June 2018

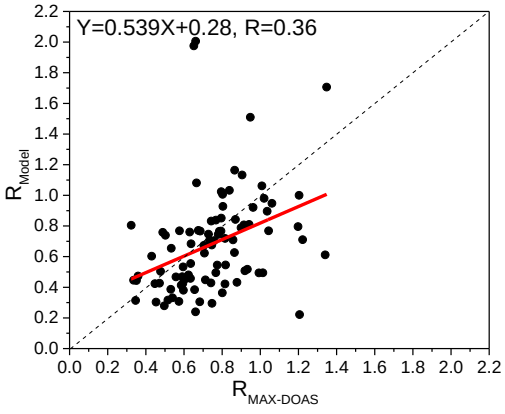

Figure 15: Scatter plots and linear regression of R_{Model} against $R_{MAX\text{-}DOAS}$ (see the text).